Plasma – Assisted Growth of MnO_2 Nanostructures for Sensing Application

Plasma – Assisted Growth of MnO_2 Nanostructures for Sensing Application

Muzahim A. A. Al.amery [1], Asmiet Ramizy , Najat A.Dahham [2]

Tikrit University/College of Science/Department of Physics [1], Tikrit University/College of Science/Department of Physics [2]

Emails: Mozahimalamery@gmail.com , dr.najat1970@tu.edu.iq

Abstract.

The limited research based on the prepare of a MnO_2 gas sensor on silicon and the testing of its sensitivity to targeted gases such as the CO_2 gas adopted in this work has led us to prepare and prepare such important sensors in human daily life. Initially, three different co2 concentrations were selected: (1.49ppm, 5.8ppm, 21.8ppm) we found that the best allergic (S = 98.28) was from the focus share (21.8ppm). This focus was worked and we also studied the amount of allergic to different temperatures 50.10° and the response time and recovery time were set for both thermal degrees, the best sensitivity was (97.22) for the sensitivity of the gas manufactured from porous silicon at a temperature (100°) C) With a short response time of (10.21sec) and a shorter recovery time at (9.1sec) all this work after the thin membrane was deposited on a slice of porous silicon type n and performed visual tests represented by UV-vis that showed that emissions occurred in the region Ultraviolet close to the electromagnetic spectrum and the optical energy gap was identified using this technique was equivalent to 3.88eV. The photosynthesis technology showed a clear peak at 324nm wavelength. There was a significant convergence in the amount of the optical energy gap calculated by this technique of 3.73nm compared to the value of the optical power gap resulting from UV-vis, which was equal to 3.88eV. The results of the Raman spectroscopy test confirmed the acquisition of the thin four-angle MnO_2 membranes resulting from the vibration of one type of atoms, as the displacement of Raman appeared at the highest intensity corresponding to the wavenumber of these thin membranes 512cm-1. The synthetic examinations represented by both the atomic force microscope for the study of the topography of the thin membrane recorded proved that the thin membrane is characterized by high roughness and granular vertical growth, and the square root of the square of the average roughness square has been calculated, granular volume rate 30.68nm, deviation 6.768nm, increase in surface area 4.446nm, surface thickness 46.78nm and this large surface roughness of the membrane surface has increased the sensitivity of the gas sensor. Then came the role of using FESEM technicians, the results of which came after the tests that the membrane is characterized by the dense random and compressed distribution of semi-spherical nanoparticles and a nanosize rate of about 33.58nm using ImageJ. Finally, the pattern of x-ray diffraction that the membrane formed with a quadruple-angle, monolithic and high-crystallization composition, the degree of crystallization was 70.25, and the granular size was found according to Shearer's image from the pattern data of the pattern of the dehydration has been calculated and is equivalent to 31.81nm.

Keywords: MnO_2, Porous Silicon, Photoluminescence, FESEM, gas sensor.

1. Introduction

Crystal structure Nanoparticles of any material acquire a very small size to be within the range of the nanoscale range. This small nanoscale imparts many properties and applications for that material and

makes it have unique properties that distinguish it from the bulk size of the material[1]. One of the most promising semiconducting metal oxides MnO_2[2]. MnO_2 possesses properties in nanoscale extremely important and unique in many applications such as Treatment of hazardous waste, medical preparations, lithium batteries, treatment of pure water and wastewater, antibacterial, electrochemical capacitors, Solar cells, and gas sensors[3]–[6]. Manganese oxide (MnO_2 can be prepared in multiform one dimensional (1D) nanoscale form include nanoparticles, nanowires, and nanotubes, Two dimensional (2D) include nanoparticles and nanoscale films, Three dimensional (3D) includes nanostructures [7]. Fig1, shows Crystal structures of MnO_2 include λ - MnO_2 (Layered or Byrnside), δ - MnO_2 (Birnessite), γ - MnO_2 (Nsutite), R - MnO_2 (Ramsdellite). β - MnO_2 (Pyrolusite) and α - MnO_2 (Hollandite)[8],[9]. So we can be prepared it using manganese nitrate salts, potassium permanganate, and manganese acetate[10],[11]. A gas sensor is a device whose properties change such as electrical conductivity or electrical capacitance when exposed to a specific gas, this change in sensor properties, and a typical gas sensor consists of a sensitive sensor layer integrated with the transducing platform that is in direct contact with the flowing gas. The change in the physical or chemical properties occurs when the chemical reaction occurs between the gas molecules and the sensitive sensor layer, and that change in properties can be measured and analyzed through the transformer as an external electrical signal[12]. Temperatures effect of the mechanism metal oxide gas sensors range from (200 – 450 °C)[13]. Gas sensor characteristics depend on the average grain size and porous structure for example, the sensitivity increases when the nanoparticles have small average grain size, and this will decrease the temperature and save energy this can be achieved through the use of crystalline materials, and this is the goal of most researchers interested in gas sensors[14],[15]. In this study, Plasma - assisted in the preparation of MnO_2 nanoparticles solution for MnO_2 thin films deposition on Porous Silicon slide. The optical and structural examinations were performed using some of the techniques included UV-vis, Photolumenisece (PL), Raman Spectroscopy, XRD, AFM and FESEM. To study the structural and optical properties of thin film deposition, determine the emission spectra, calculate the optical energy gap of MnO_2 films, describe the topography and morphology of the thin film surfaces using these techniques, and then use the thin film as an electrode in the gas detector system and measure the sensitivity.

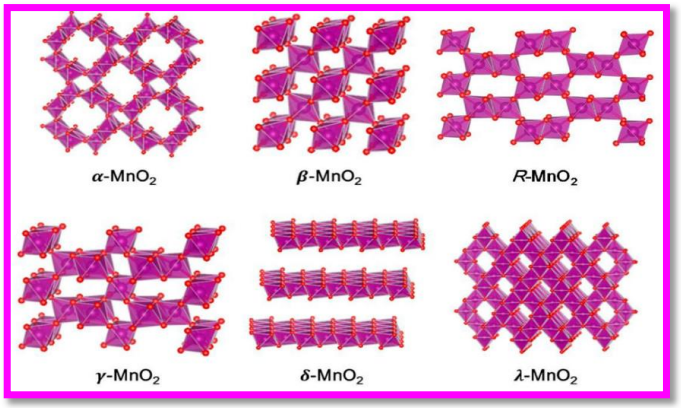

Fig.1:
Crystal structures of MnO_2[8],[9]

2. Experiment Details

2.1. Synthesis of MnO_2

The solution was prepared using manganese nitrate salts $Mn(NO_3)_2$ at room temperature 30°C and Molarity 0.4M by dissolving 1.0737g from the substance in (15ml) from distilled water using a magnetic stirrer for a period of 15min without heat, and during the dissolution process, drops of NaOH were added until the acidity of the solution reached PH = 10 by PH-meter, Plasma system was used to obtain the nanoparticles of the prepared solution for 15min, the color change was monitored until we reached the desired reddish-brown. MnO_2 thin films deposited to five-layer on Porous Silicon slide by used spin

coating. Spin speed was 1500rpm and spin time 2 min selected. Dry the thin film by using a magnetic stirrer at a temperature of 70°C for 5min.

3. Results and Discussion

3.1. UV– vis Spectrum

Perform this check using a UV-vis spectrum device produced by INOVI LAB and manufactured in the United Kingdom. Ultraviolet-visible spectroscopy obtains the absorption spectrum of compounds. In actuality this absorption of light energy or electromagnetic radiation. UV-vis scan results at range 200 – 700nm at temperature room 30°C and graph the relationship between (hυ) and $(\alpha h\upsilon)^2$, and optical gap of the drawing is equal to E_g = 3.88eV as shown as in fig.2, It is within the optical energy gap range of the semiconductors and that value is due to the high absorption peak that appeared at the wavelength 360nm, this range corresponds to the UV region and this absorption peak is largely. The result was an amount in good agreement with the findings of the researcher JS Sherine[16], but the method of preparing the thin films differed from it.

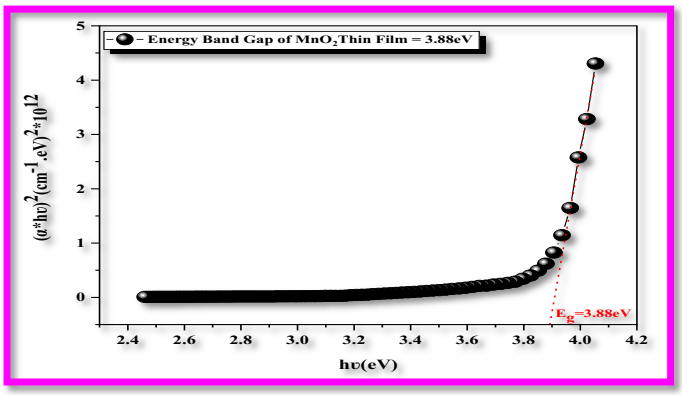

Fig.2: Optical band gap of MnO_2 thin film

3.2. Photoluminces (PL) Spectrum

The Spectrometer Fluorescence System used a Flouromate FS-2 Spectrometer. The light source used was 150W Continuous-wave Xenon - Arc Lamp and the wavelength of the light used for excitation and emission was within the range 190 - 900nm. Photoluminescence is the optical phenomenon that causes the emission of incandescent light when irradiating the materials. PL is applied to semiconductors for purpose of identifying the purity of the semiconductors. Photoluminescence is a method for sensing the electronic structure of materials by studying and analyzing the light radiation produced by fluorescent. Well used to optical band gap determination and Exposure to crystal defects optical energy gap determination [17]–[23]. Using a device FS-2 Spectrometer. The light source used was 150W continuous wave Xenon - Arc Lamp and the wavelength of light used for excitation and emission was within the range 190 - 900nm. The results showed the peak at the wavelength of 328nm in fig.3 indicating the emission of the luminescence spectra in green-blue violet at that wavelength corresponding to the near-ultraviolet spectral region. The waveform indicates that the crystal structure of the prepared thin film has a structural structure β - MnO_2 or Pyrolusite.

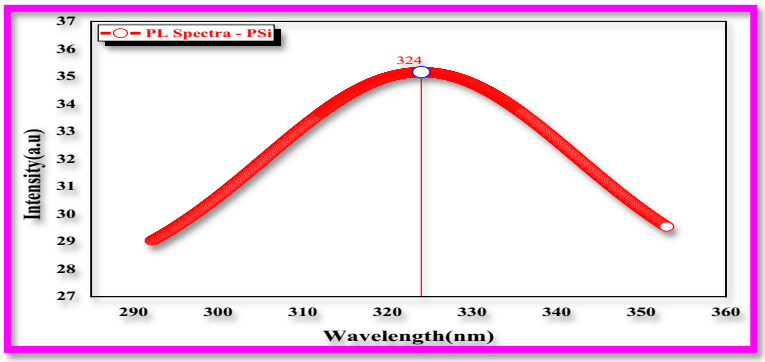

Fig.3: Photoluminces (PL) Spectrum for MnO_2

The amount of the optical energy gap is equal to 3.59eV, as shown in fig.4. Almost identical to the optical energy gap values obtained from UV - Vis Spec.

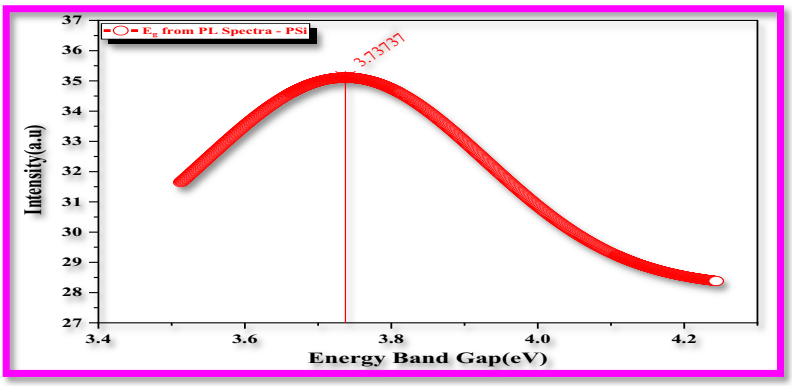

Fig.4: optical energy gap for MnO_2 calculated from PL spec.

3.3. Raman Spectroscopy

Raman spectroscopy was performed to study the patterns of low-frequency molecular vibrations and to reveal the crystal structure. In this analysis, the spectral system is used, in the operational mode CW, using a light source of wavelength 532nm and electric power of 20mW. Raman spectroscopy is a method of molecular vibrational spectroscopy that uses the principle of the interaction of a laser beam with matter to provide information on the vibrations that occur to the particles of a substance. In this analysis, the operational mode and the light source have a wavelength of 532nm and electrical power. From fig.5 confirms that the Raman shift occurred at the wavenumbers 433,512and 619cm^{-1} respectively. The highest intensity appeared at the peak of 512cm^{-1}, resulting from the symmetric stretching vibrations between one type of atoms, these symmetric stretching vibrations are a perpendicular expansion to the octahedral direction MnO_6 within a quadrangular frame associated with the tunnel type (2 * 2) which represents the crystal structure MnO_2. The lower intensity peak corresponding to the wavenumber 433cm^{-1} and 619cm^{-1} due to symmetric stretching vibrations between two different types of atoms O - M - O; this supports the formation of MnO_2 Tetragonal.

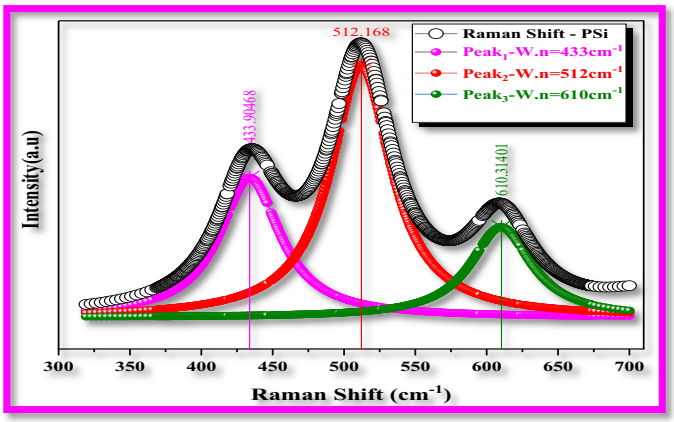

Fig.5: Raman spectrum of thin-film prepared on a Porous silicon slide.

3.4. AFM and FESEM

The device used to perform the inspection is TT-2 AFM Workshop. This technique used to identify the topography of thin-film surfaces prepared on Porous Silicon slides with five layers of deposition. The device TT-2 AFM Workshop was used in this work. The scanning range of the images obtained from the atomic force microscopy came in dimensions 78nm*78nmm. Fig.6 shows the surface topography by RMS roughness of 6.086nm and average grain size of 30.68nm. From the above we conclude that the surfaces of the films deposited on the porous silicon slide have higher roughness with long granules, meaning that the granular growth was vertical and since the increase in the surface roughness of the thin film leads to a decrease in the size of the granules, which in turn increases the sensitivity of the gas sensor. Therefore, these films can be used in multiple applications. The thinner thin film is coarser and less granular to be used as a gas sensor[24].

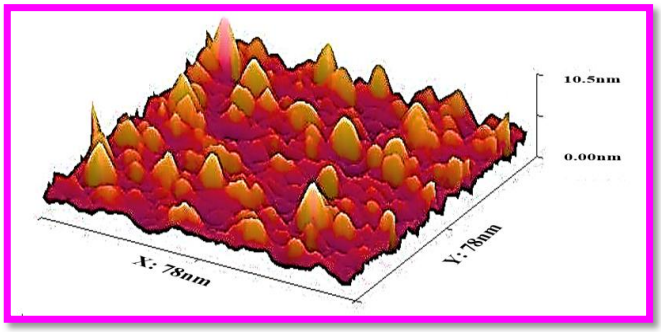

Fig.6:AFM image of MnO_2 thin film sample.

Thin-film morphology or the method of arranging the nanoparticles plays a major role in increasing the electrochemical reaction. Thus, the sensitivity of the gas sensor increases by using it as an electrode[25]. FESEM tests were performed using the ZEISS SIGMA VP system. FESEM showed the morphology of the MnO_2 thin film on the porous silicon chip in a high-magnification scan range ((100nm) (look fig.7).

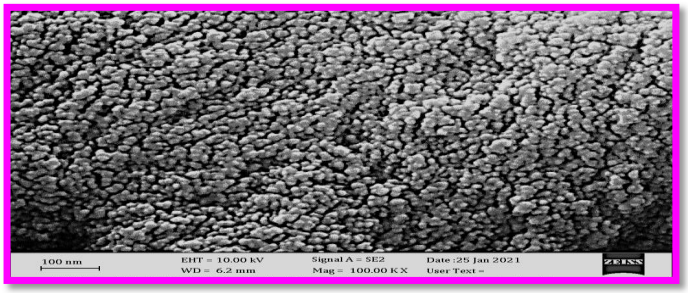

Fig.7: Morphology of MnO_2 thin film on porous silicon slide.

The diameter of the nanoparticles (grain size) was calculated by using ImageJ software, and the diameter of the grains ranged between (20 - 35nm). The average diameter of the nanoparticles is found to be equal to (33.58nm), which corresponds to the resulting grain size for examining the atomic force microscopy (AFM) as shown in fig.8. A). graph of the histogram distribution of sizes at scan range (100nm). B) Average diameter of nanoparticles.

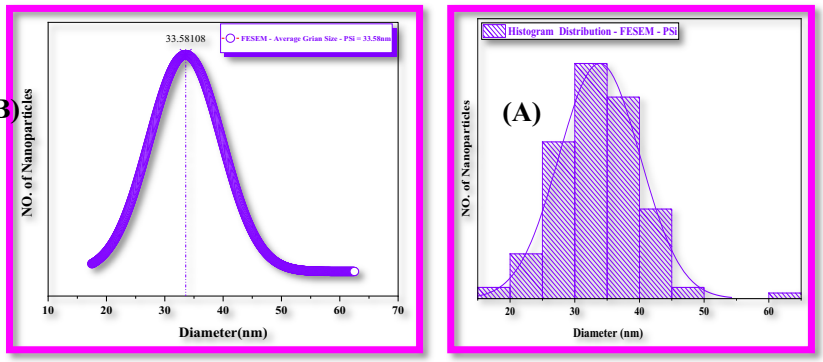

Fig.8:(A) Histogram distribution of nanoparticles diameter. (B) The average diameter of nanoparticles.

3.5. X-Ray Diffraction (XRD)

X-ray diffraction (XRD) tests were performed using the Panalytical X'Pert Pro system shown in Fig.9. According to the following parameters, Generator Settings 40 mA, 40 kV, Anode Material: Cu Wavelength X-Ray Source λ = 0.15406nm. This technique is used to identify the crystal structure of the prepared thin film. The diagnostic results of the XRD Diffraction technique of MnO_2 films prepared on a porous silicon chip showed that the crystal system for the thin film is of the tetragonal type. In general, the other crystalline parameters after matching the diffraction peaks that appeared in the X-ray diffraction data with the International Center for Diffraction Data (ICDD) diffraction peaks (00-044-0141) were according to the following specifications shown in Table 1.

Table.1: Crystalline parameters of MnO_2 thin films according to (ICDD = 00 - 044 - 0141)

No.	**Crystallographic Parameters**			
1.	name	Manganese Oxide		
2.	Mineral name	Birnessite, syn		
3.	Crystal system	Tetragonal		
4.	Space group	14/m		
5.	Space group number	87		
6.	Empirical formula	MnO_2		
7.	Chemical formula	MnO_2		

8.	Cell Parameters	Lattice Const.	a = b (A°)	9.784
			c (A°)	2.863
		angle between lattice vectors	α = β = γ (°)	90

As the peaks were cleared at the sites and levels corresponding to them that represent Miller's index as shown in the table.2:

Table 2: Positions of the peaks of the XRD pattern, and corresponding Miller levels.

No. of Peak	**Pos. (20°)**	**Miller level (h k l)**
1.	12.78139	(1 1 0)
2.	18.11117	(2 0 0)
3.	25.70346	(2 2 0)
4.	28.84861	(3 1 0)
5.	37.53423	(2 1 1)
6.	39.01486	(3 3 0)
7.	41.20515	(4 2 0)
8.	41.96695	(3 0 1)
9.	46.03551	(3 2 1)
10.	47.38699	(5 1 0)
11.	49.90946	(4 1 1)
12.	52.86146	(4 4 0)
13.	56.93023	(4 3 1)
14.	60.25753	(3 1 0)
15.	68.20662	(2 0 2)
16.	69.71984	(5 4 1)
17.	71.19279	(2 2 2)
18.	72.71166	(3 1 2)
19.	77.15767	(4 0 2)
20.	78.58762	(3 3 2)

X-ray diffraction pattern is well matched in location and intensity JCPDS # 44-0141 and the MnO_2 thin film has a tetragonal crystal system according to the fig.6 since the information in Table.2 for the positions of the diffraction peaks in addition to Miller indicators prove that the MnO_2 thin film is well crystallized and pure.

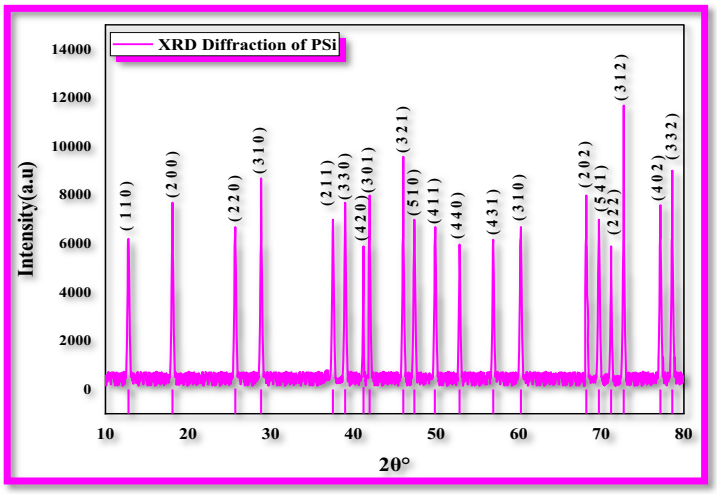

Fig.9:
X-ray diffraction of the MnO_2 thin film on a porous silicon slide.

The average grain size found by using X-ray diffraction data (XRD data) is equal to 31,85nm as shown in table.2 by using Scherer's formula it's given as[26]:

$$D = \frac{k\lambda}{\beta cos\theta} \dots\dots\dots 1$$

Where:

D: grain size in units (nm).

k: Shearer's constant and its value (0.9).

λ: the source X-ray wavelength and its value (0.15406 nm).

β: FWHM in units (Radians).

θ: the location of the peak appearing in the X-ray diffraction pattern in radians.

The average grain size as follows shown in table 3:

Table 3: The crystalline grain size of MnO_2 from X-ray diffraction data (XRD data).

No. of Peak	Pos. (2θ°)	FWHM.(2θ°)	Grain Size D (nm)
1.	12.78139	0.2511	31.8357763
2.	18.11117	0.25337	
3.	25.70346	0.25938	
4.	28.84861	0.24777	
5.	37.53423	0.25478	
6.	39.01486	0.24568	
7.	41.20515	0.11993	
8.	41.96695	0.20503	
9.	46.03551	0.24153	

10.	47.38699	0.25689	
11.	49.90946	0.25923	
12.	52.86146	0.21261	
13.	56.93023	0.22841	
14.	60.25753	0.25861	
15.	68.20662	0.22942	
16.	69.71984	0.25924	
17.	71.19279	0.19308	
18.	72.71166	0.22854	
19.	77.15767	0.25498	
20.	78.58762	0.24614	

The crystallinity degree in table 4 also calculated from the X-ray diffraction data using the relationship[27]:

$$\text{Crystallinity} = \left(\frac{\text{Area of Crystalline Peaks}}{\text{Area if } All \text{ Peaks}}\right) \times 100\% \dots\dots\dots 2$$

We can deduce from the AFM, FESEM, and XRD tests the convergence and consistency of the average grain size is very large. The degree of Crystallinity of the MnO_2 thin films deposited on the porous silicon slide calculated as shown in the table.3. Crystallization refers to the degree to which the structure is arranged and there are no crystalline defects, and there is virtually no overlap in solid matter. In crystals, atoms or molecules are arranged regularly and periodically. Crystallization has a significant impact on rigidity, intensity, transparency, and proliferation.

Table 4: Crystallinity degree of MnO_2 thin films from X-ray diffraction data (XRD data).

No. of Peak	**Area of Crystalline Each Peak**	**Sum. Area of Crystalline Peaks (counts × 2θ°)**	**Area of all Peaks (counts × 2θ°)**	**Crystallinity**
1.	2571.51701	44721.43386	63659.06782	70.2514746
2.	2503.90485			
3.	2337.41299			
4.	2641.59959			
5.	2625.57137			
6.	2356.15651			
7.	951.51081			
8.	1939.8807			
9.	2261.03074			
10.	2208.82242			
11.	2573.79781			
12.	1803.66283			
13.	2192.26322			
14.	2426.41954			
15.	1806.07675			
16.	231.83695			
17.	2347.66412			

18.	1424.56981			
19.	2379.0085			
20.	2615.58826			

3.6. Characters of Gas Sensor

Gas sensors manufactured from semiconductors were generally characterized by high sensitivity[28]. CO_2 gas, which is an oxidizing gas, was used[29] in studying the properties of the gas sensor manufactured from MnO_2 films and prepared on a porous silicon slide of three different concentrations (1.49, 5.8, and 21.8ppm.) Of carbon dioxide (CO_2), and it was found that the best sensitivity was at a concentration of (21.8ppm) and a sensitivity of (S = 98.28), as shown in Fig.10, From the aforementioned figure, we deduce the change of the sensitivity and the response time when the target gas concentration changes from zero for a specific purpose. The sensitivity increased with the increase in the gas concentration due to the increase in the surface interactions of the membrane with the target gas, which reduces the resistance of the sensor and increases the conductivity.

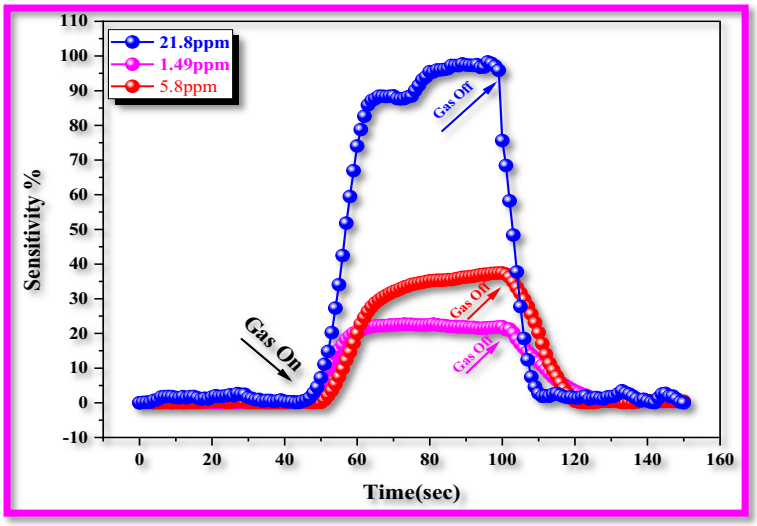

Fig.10: The sensitivity changes with the concentration of the best response to the gaseous sensor electrode manufactured on the porous silicon slide.

After that, the target gas concentration was fixed at (21.8ppm), which obtained the best sensitivity and temperature change at 50 and 100°C. Properties of the gas sensor were studied, represented by the response time, recovery time, and the response time of the sensor to the target gas at that concentration and those temperature degrees of the porous silicon sensor as shown in Fig.11

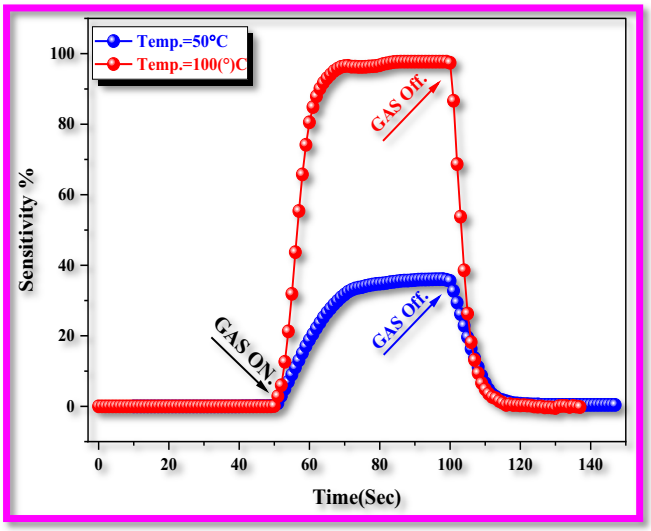

Fig.11: The sensitivity change with temperature for the best response to the gaseous sensor electrode manufactured on the porous silicon slide.

At 50 °C the sensitivity was (S = 36.08) and (t_{res} = 15.79, t_{rec} = 9.1sec) to the gaseous sensor prepared on the porous silicon slide so at a temperature of 100 °C the amount of sensitivity is (S = 97.72) and t_{res} = 10.21, t_{rec} = 9.1sec as shown in Fig.12A and 12B respectively**.** Table.4 shows the sensitivity, response, and recovery times at a concentration of (21.8ppm) and the temperatures at which the gaseous sensor properties of the porous silicon sensor.

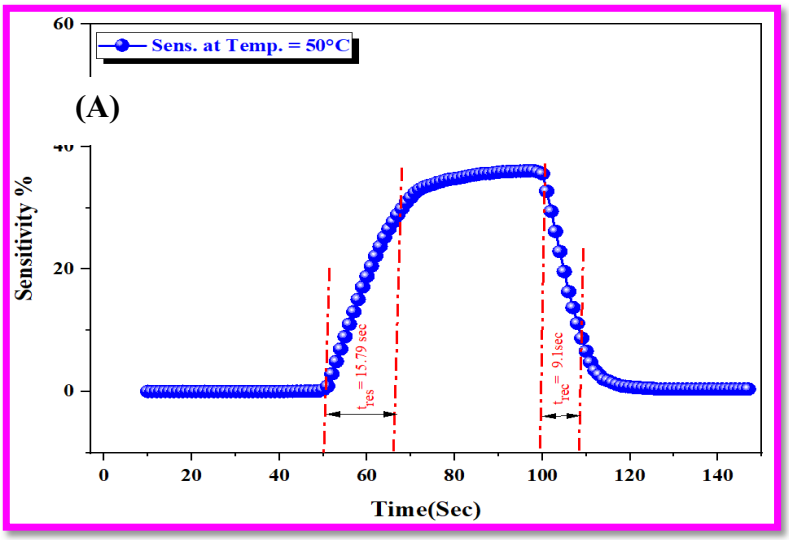

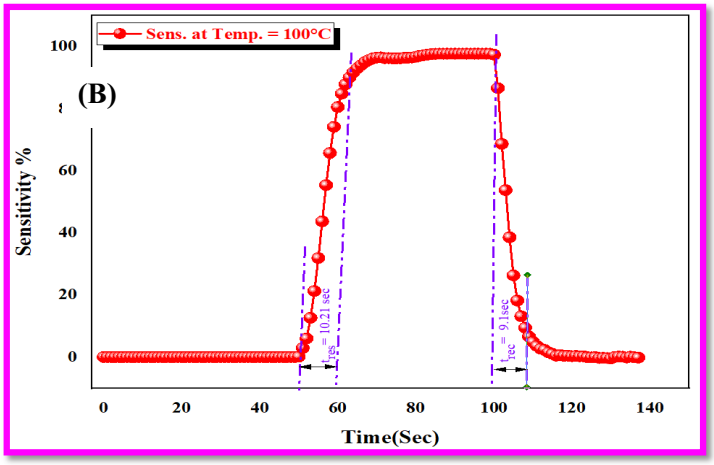

Fig.12: The sensitivity and the response times and recovery of the prepared sensor electrode at a temperature: (A) 50°C, (B) 100°C

Table5: Sensitivity, response time, and recovery time values at temp. (50°C,100°C)

Sample	Temp. (°C)	Sensitivity (%)	Response Time (sec)	Recovery Time (sec)
Porous Silicon	50	36.08	15.79	9.1
	100	97.22	10.21	9.1

Conclusion:

We were able to synthesize manganese dioxide nanoparticles of granular size within the nanoscale range of 30nm and prove that the manganese dioxide compound possesses a direct energy gap according to the UV-vis assays. The results of the PL assays showed clear peaks in the wavelength range 324nm, that the blue-green photoluminescence emission spectrum at those wavelengths corresponding to the near-ultraviolet spectral region, and this indicates that the crystal structure of MnO_2 is tetragonal. The amount of the energy gap for these membranes was calculated and depending on the wavelengths, and it was found that it is equal to 3.73eV. It was observed that the Raman shift appeared at the wavenumbers 433, 512, 619 cm^{-1} respectively. The highest intensity was at the wavenumber 512cm^{-1}. The results of the AFM assays were with the following parameters Average Grain Size = 30nm, Roughness Average = 6.086nm, Surface Thickness = 46.78nm, Surface Area Increase = 4.446nm, and Skewness = 6.768nm. FESEM assay also revealed the morphology of the MnO_2 thin film, the compact and random dense distribution of the aspherical nanoparticles of different sizes without the appearance of other formations. XRD diagnostic results indicated that the crystalline membrane system is of the tetragonal type. Grain size 31.83nm was found based on XRD data using Scherer's formula and Crystallinity Degree = 70.25 was also calculated. the manufacture of a secondary sensor for the thin MnO_2 films for CO_2 gas at a concentration of 21.8ppm with high sensitivity and short response time At a temperature of 100°C and better than its sensitivity at low temperatures 50°C.

References:

[1] A. M. Toufiq, F. Wang, Q. U. A. Javed, Q. Li, en Y. Li, "Photoluminescence spectra and magnetic properties of hydrothermally synthesized MnO_2 nanorods", Mod. Phys. Lett. B, vol 27, no 29, bll 1–8, 2013, doi: 10.1142/S0217984913502114.

[2] L. Bigiani, D. Zappa, C. Maccato, E. Comini, D. Barreca, en A. Gasparotto, "Quasi-1D MnO_2

nanocomposites as gas sensors for hazardous chemicals", Appl. Surf. Sci., vol 512, no February, bl 145667, 2020.

[3] J. Rinita, R. Jose, en N. S. N. Jothi, "Acclimated growth and characterization of manganese oxide nanospheres using natural extract from trigonella foenum-graecum", Mater. Technol., vol 00, no 00, bll 1–8, 2020, doi: 10.1080/10667857.2020.1761660.

[4] K. Seki en W. Mori, "Syntheses and Characterization of Microporous Coordination Polymers with Open Frameworks", J. Phys. Chem. B, vol 106, no 6, bll 1380–1385, Feb 2002, doi: 10.1021/jp0130416.

[5] Y. S. Rammah, A. S. Abouhaswa, A. H. Salama, en R. El-Mallawany, "Optical, magnetic characterization, and gamma-ray interactions for borate glasses using XCOM program", J. Theor. Appl. Phys., vol 13, no 2, bll 155–164, 2019, doi: 10.1007/s40094-019-0331-6.

[6] P. Katsoufis et al., "Study of a thin film aluminum-air battery", Energies, vol 13, no 6, bll 1–9, 2020, doi: 10.3390/en13061447.

[7] P. T. Anastas en M. M. Kirchhoff, "Origins, current status, and future challenges of green chemistry", Acc. Chem. Res., vol 35, no 9, bll 686–694, 2002, doi: 10.1021/ar010065m.

[8] J. Shin, J. K. Seo, R. Yaylian, A. Huang, en Y. S. Meng, "A review on mechanistic understanding of MnO_2 in aqueous electrolyte for electrical energy storage systems", vol 6608, 2019, doi: 10.1080/09506608.2019.1653520.

[9] G. H. Nail, "Synthesis and Study the Properties of PANI/MnO_2 Conductive Nano Composites", Master Thesis / Univ. Anbar / Coll. Sci. / Dep. Chem., 2020.

[10] M. Wu et al., "Manganese dioxide nanosheets: From preparation to biomedical applications", Int. J. Nanomedicine, vol 14, bll 4781–4800, 2019, doi: 10.2147/IJN.S207666.

[11] P. Hou, L. Dong, L. Cai, en Z. Chen, "Manganese dioxide nanosheets : from preparation to biomedical applications", 2019.

[12] G. Korotcenkov, . "Metal Oxides for Solid-State Gas Sensors: What Determines Our Choice? Mater. Sci. Eng. B139, pp 1-23", 2007.

[13] N. M. and N. Y. C. Xu, J. Tamaki, "Correlation between gas sensitivity and crystallite size in porous SnO_2-based sensors.," Chem. Lett., no. 3", Sensors Actuators B. Chem., bll 441–444, 1990.

[14] A. R. and Y. Komem, "The effect of grain size on the sensitivity of nanocrystalline metal-oxide gas sensors", Fac. Mater. Eng. Tech. Inst. Technol., vol 95, 2004.

[15] H. H. N. Ali, "Synthesis, Characterization and Gas Sensor Performance of In2O3 – Ag_xO nano Composites Prepared by Chemical Bath Deposition", Master Sci. PhysicsThesis ,University Anbar, 2016.

[16] J. S. Sherin, M. Haris, D. S. Manoj, J. Koshy, en J. K. Thomas, "Enhanced electrochemical properties in nanostructured β - MnO_2 , synthesized through a single step auto-igniting modified combustion technique", vol 10, no 3, bll 647–655, 2017.

[17] T. Hayashi, N. Bonnet-Mercier, A. Yamaguchi, K. Suetsugu, en R. Nakamura, "Electrochemical characterization of manganese oxides as a water oxidation catalyst in proton exchange membrane electrolysers", R. Soc. Open Sci., vol 6, no 5, 2019, doi: 10.1098/rsos.190122.

[18] S. Akbari, M. M. Foroughi, en M. Ranjbar, "Nanomedicine & Nanotechnology Solvent-free Synthesis and Characterization of MnO_2 Nanostructures and Investigation of Optical Properties", vol 9, no 3, bll 3–7, 2018, doi: 10.4172/2157-7439.1000498.

[19] Y. Zhao en G. Zhu, "A technology of preparing MnO_2 nanowire from the low grade manganese ore", vol 3, no 1, bll 27–32, 2019.

[20] V. B. J. S.C. Vella Durai, E. Kumar, D. Muthuraj, "Investigation on Electrical and Structural Properties of Manganese Dioxide Nanoparticles", vol 12, no 3, bll 4–8, 2020.

[21] E. Kareem Jassem, A. Mustafa Abdul Majeed, en N. Mossa Umran, "The Effect of Temperature on Structural and optical properties of Manganese Oxide Nanoparticles", J. Phys. Conf. Ser., vol 1279, no 1, 2019, doi: 10.1088/1742-6596/1279/1/012004.

[22] N. Rajamanickam, S. Rajashabala, en K. Ramachandran, "Structural and Optical Properties of alpha-MnO_2 Nanowires and beta-MnO_2 Nanorods", 2014, doi: 10.1063/1.4872568.

[23] P. A. Shinde en S. Korea, "Hydrothermal synthesis of manganese oxide thin films using different oxidizing agents for supercapacitor application", vol 10, no 1, bll 532–537, 2017.

[24] D. Barreca, A. Gasparotto, F. Gri, E. Comini, en C. Maccato, "Plasma-Assisted Growth of β-

MnO_2 Nanosystems as Gas Sensors for Safety and Food Industry Applications", Adv. Mater. Interfaces, 2018.

[25] N. R. Chodankar, G. S. Gund, en D. P. Dubal, "Alcohol mediated growth of α -MnO_2 thin films from $KMnO_4$ precursor for high performance supercapacitors", 2014, doi: 10.1039/C4RA09268F.

[26] H. H. N. Ali, "Synthesis, Characterization and Gas Sensor Performance of In_2O_3 – Ag_xO nano Composites Prepared by Chemical Bath Deposition", MS.C Sci. Phys. Univ. Anbar Dep. Phys., 2016.

[27] S. Prepared, B. Khoshnevisan, B. Marami, M. Farahmandjou, en Y. Bone, "X-ray diffraction and infrared spectroscopy analyses on the crystallinity of engineered biological hydroxyapatite for medical application", 2020, doi: 10.1088/1757-899X/79/1/012028.

[28] Z. Jing, X. U. Longjun, en X. I. E. Chao, "Preparation of chemical manganese dioxide from low-grade rhodochrosite ore", bll 380–384, 2013, doi: 10.1007/s11631-013-0645-z.

[29] E. Environ, M. B. Ansari, en S. Park, "Environmental Science MINIREVIEW Carbon dioxide utilization as a soft oxidant and promoter in catalysis †", bll 9419–9437, 2012, doi: 10.1039/c2ee22409g.